Int J Adv Manuf Technol (2017) 92:3299–3309
DOI 10.1007/s00170-017-0419-6

ORIGINAL ARTICLE

An experimental and numerical investigation on the formability of AA7075 sheet in hot stamping condition

Wenchao Xiao[1] · **Baoyu Wang**[1] · **Kailun Zheng**[2]

Received: 11 January 2017 / Accepted: 10 April 2017 / Published online: 21 April 2017

Abstract Formability of aluminum alloys at elevated temperatures are of vital importance to process design and numerical simulation of aluminum hot stamping. In this paper, the hot formability of AA7075 was investigated experimentally and numerically. Firstly, a series of hot uniaxial tensile tests were performed on a Gleeble 3500 thermomechanical simulator to determine constitutive relationships of AA7075 at different temperatures and strain rates. Based on these results, a uniaxial damage model was established, and further extended to a multi-axial continuum damage mechanics (CDM) based model with the consideration of stress state and strain path effects for hot stamping. Good agreement between model fitting and experimental results was achieved. Secondly, hot formability tests were conducted to investigate deformation characteristics at elevated temperatures. Finally, a finite element (FE) model using software ABAQUS with implemented the CDM model via subroutine was established and validated by corresponding experimentations. The developed FE model was utilized to investigate effects of process variables on material deformation and damage evolution in detail. It was found that formability can be improved with decreasing forming temperature and increasing forming speed. In addition, friction has a dominant effect on determining failure location.

Keywords Continuum damage mechanics (CDM) · Damage · Hot stamping · Formability · AA7075

✉ Baoyu Wang
bywang@ustb.edu.cn

[1] School of Mechanical Engineering, University of Science and Technology Beijing, Beijing 100083, China

[2] Department of Mechanical Engineering, Imperial College London, SW72AZ, London, UK

1 Introduction

Higher requirements have been raised by the automotive industry for achieving the goal of light-weight due to the urgent demand of improving fuel efficiency and reducing pollution [1, 2]. Aluminum alloys have the merits of high specific strength, good impact and corrosion resistance, and rich in resources, which make them to be an ideal material candidate for automotive Original Equipment Manufacturers (OEMs). AA7075, as a typical high strength 7xxx series aluminum alloy, is gaining popularity to be used to manufacture structural components in a car body. However, the poor ductility of AA7075 and serious spring-back in cold stamping restrict the applications in manufacturing complex-shape components. To address above drawbacks, a patented hot stamping process for aluminum alloys, solution Heat treatment, cold die Forming and Quenching, (HFQ®), [3–5] was proposed and regarded as a leading technology. In HFQ®, heat treatment for alloy strengthening and hot stamping for component manufacturing are integrated in one operation, which can guarantee the dimensional accuracy and reduce the overall cost. In the meantime, forming at elevated temperatures increases alloy ductility significantly making it achievable for forming complex-shaped components.

Formability of aluminum alloys at elevated temperatures determined the capability of HFQ®. Many researchers have investigated formability of aluminum alloys in hot forming condition extensively. Wang et al. [6] studied effects of blank temperature and stamping speed on the formability of hot stamping AA2024. It has been found that formability increased with increasing temperature up to 450 °C, followed by a sharp decrease with a further temperature raise. The formability reduction is believed to be caused by the softening of grain boundaries by solute enrichment and softening of the matrix around inclusion particles. Fakir et al. [3] numerically

investigated the formability of AA5754 in HFQ®. Effects of forming temperature and speed on the thickness uniformity were studied, the results have shown that a higher forming speed enabled to improve hot formability of AA5754. Zhou et al. [7] used an optimization method to study the influence of process parameters on the formability of AA6111 for hot stamping an anti-collision side beam structure inside car doors, and found that the non-dominated sorting genetic algorithm II (NSGA-II) optimization procedure enabled to obtain optimum process parameters for maximizing formability. Based on above discussions, temperature and stamping speed are two critical factors influencing the formability for hot forming. However, their effects on the formability of high strength AA7075 sheets lack thorough investigations to date.

Finite element (FE) method is a robust approach to evaluate feasibility and potential of hot stamping components [8]. To model the constitutive relationships of alloy at elevated temperatures precisely, advanced material modelling with the consideration of the viscoplastic flow behavior [9, 10], dislocation evolution and damage [11–13] is essential. Wu et al. [14] investigated the flow behavior of AA7050 using hot compression tests. The characteristics of stress strain curves were determined by the coupled influences of work hardening, dynamic recovery and dynamic recrystallization. Ma et al. [15] studied the damage evolution of AA6111 during hot deformation using hot tensile tests, and found that the occurrence of damage was mainly caused by the nucleation, growth, and coalescence of micro-voids. A damage constitutive model for AA6111 was established based on the damage evolution. For hot stamping aluminum alloys, Lin et al. [16] proposed a unified dislocation-driven based viscoplastic material model. Using this model, Fakir et al. [3] and Mohamed et al. [4] established constitutive models for AA5754 and AA6082, respectively. Good agreements have been observed between the fitting and hot uniaxial tensile results. Furthermore, Lin et al. [17] proposed a novel continuum damage mechanics (CDM) model based on the plane stress assumption, which enables to predict the shapes of forming limit curves (FLCs) for aluminum alloys under hot stamping condition. In this model, material failure was considered as the accumulation of micro-damage. Shao et al. [18] has developed a new design enabling to determine FLCs of AA6082 in hot stamping. The new test rig utilized Gleeble thermos-mechanical simulator to achieve an accurate temperature and strain rate control.

To this extend, the study of constitutive modeling for hot stamping 7xxx series aluminum alloy is relatively few. In addition, the effects of stress state, strain path, temperature and strain variations were not considered. Therefore, formability and constitutive modeling for AA7075 at elevated temperatures need to be studied to evaluate the process feasibility of HFQ®. In this paper, hot uniaxial tensile tests were performed on a Gleeble 3500 thermomechanical simulator to investigate the hot tensile deformation behaviors and damage characteristics of AA7075, based on the obtained experimental results, a unified uniaxial viscoplastic damage model was developed. Furthermore, a multi-axial CDM model considering different stress state, extended from the uniaxial material model, was established. Finally, the developed CDM model was implemented into FE simulations via a user-defined subroutine to numerically assess the formability of AA7075 at elevated temperatures in detail.

2 Experimental method

2.1 Material

The material used was AA7075 in T6 condition with a thickness of 2 mm. The chemical composition is given in Table 1.

Table 1 Chemical composition of AA7075-T6

2.2 Uniaxial hot tensile tests

Uniaxial hot tensile tests were performed to obtain the stress strain behaviors and ductility performances of AA7075 at different temperatures and strain rates. Specimens were machined at the rolling direction and dimensions of specimen is shown in Fig. 1a. The gauge length with a uniform temperature distribution was 10 mm, and the width of gauge zone was 10 mm.

Fig. 1b shows the schematic temperature profile of hot tensile tests. The whole procedure can be described as follows: Initially the specimen was heated to 450°C at a rate of 20 °C/s, and further heated to the solution heat treatment (SHT) temperature, 480 °C, at a heating rate of 5 °C/s, and soaked for 600s to guarantee a sufficient dissolution of original precipitates. Then the solution heat treated specimen was quenched to the target deformation temperature at a cooling rate of 50 °C/s and soaked for 10s to achieve the uniform temperature distribution within specimen. Finally, the specimen was uniaxially stretched to fracture. The specimens were isothermally deformed at different temperatures of 400, 450, and 500 °C and different strain rates of 0.1, 1, and 10 s^{-1}. The obtained stress strain data were used for modeling the uniaxial damage constitutive relationships presented in the following section.

Table 1 Chemical composition of AA7075-T6

Element	Si	Fe	Cu	Mn	Mg	Cr	Zn	Ti	Al
Wt. %	0.07	0.22	1.4	0.04	2.2	0.19	5.4	0.02	Remain

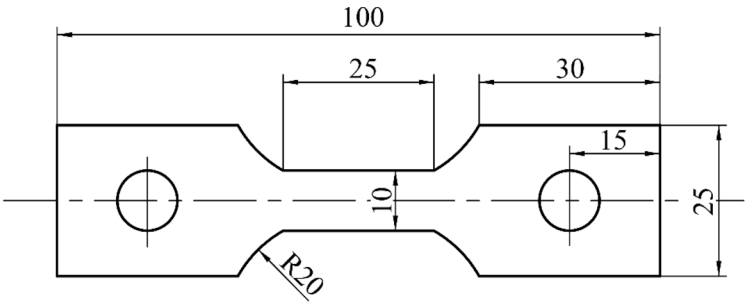

(a) Dimension of the hot uniaxial tensile specimen (all dimensions are in mm)

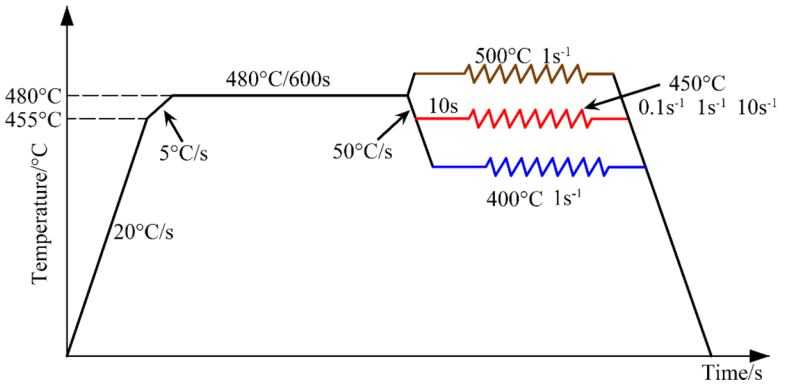

(b) Temperature profile for the hot uniaxial tensile tests

Fig. 1 Specimen design and temperature profile for the uniaxial hot tensile tests.

2.3 Hot formability tests

2.3.1 Experimental test rig and specimen design

Fig. 2 shows the experimental test rig used for determining the isothermal formability of AA7075 in hot stamping condition. The test rig was designed using a hemispherical punch with a diameter of 100 mm. To achieve an isothermal and elevated environmental temperature, heating rods were inserted into the top die and blank holder to heat the test rig to target temperatures. Thermocouples were attached in the dies and blank holder respectively to control the tool temperatures. The punch, top die and blank holder material selected stainless steel (06Cr25Ni20), with a maximum working temperature 600 °C. The whole test rig was mounted on a 60-ton hydraulic press, where the top die was fixed to the ram, and the punch was located on the machine bed, as shown in Fig. 2b.

Fig. 3 shows the geometry and dimension of specimen of hot formability tests. Specimens were cut at the rolling direction from as-received material same with those of uniaxial tensile tests, and gridding with a dimension of 2×2 mm was etched on the specimen using electrochemical corrosion for measuring principal strains.

2.3.2 Test procedure

In terms of the procedure of hot formability test, firstly, the AA7075 specimen was solution heat treated at 480 °C for 10 mins in a furnace, and the test rig was heated to deformation temperature 450 °C using the built-in heating rods simultaneously. After the solution heat treatment, the heated specimen was quickly transferred to the test rig and positioned on the blank holder. Once the specimen temperature reached the deformation temperature, the top die moved downwards and clamped the specimen with the blank holder at a constant force 6KN. The draw beads on the blank holder constricted the material flow of specimen in the flange. Then, the clamped specimen was deformed with different die strokes at a constant speed of 20 mm/s until necking occurred. Punch and the specimens were well lubricated using graphite for the contact areas. Flow chart of the hot formability tests was shown in Fig. 4.

3 Material constitutive model

3.1 Establishment of uniaxial damage model

To model the constitutive relationships of aluminum alloys, a unified dislocation-driven material model considering material hardening and dislocation recovery [16] was used. The uniaxial constitutive equations were given in Eqs. (1) to (5). To formulate the damage evolution, a continuum damage mechanics based damage formulation was used [4] to reflect the formation and accumulation of damage during the dynamic process of plastic deformation.

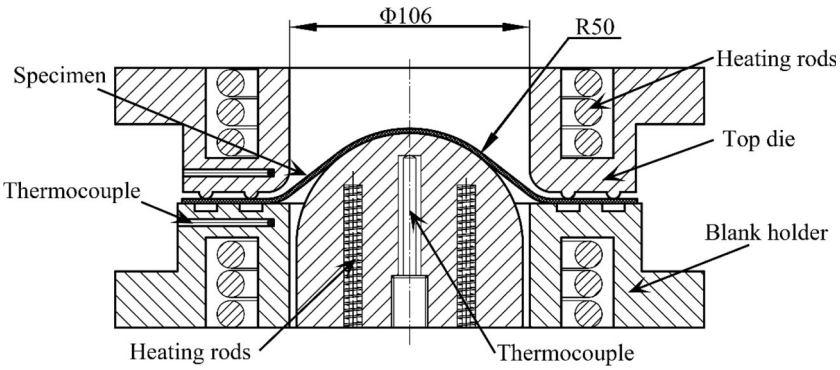

(a) Schematic of hot formability test rig (all dimensions are in mm)

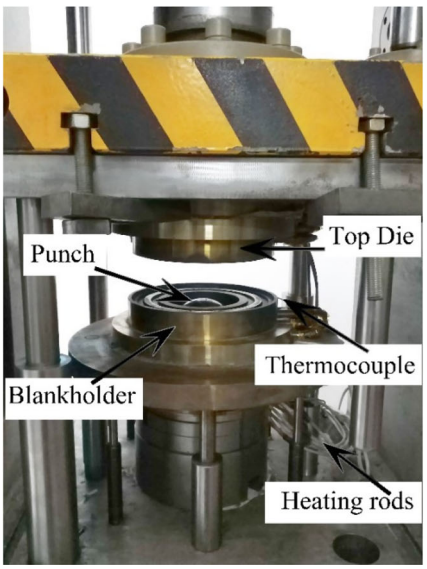

(b) Experimental test rig

Fig. 2 Experimental test rig for hot formability tests

$$\dot{\varepsilon}_p = \left(\frac{\sigma/(1-\omega)-R-k}{K}\right)^n \tag{1}$$

$$\dot{R} = 0.5B\bar{\rho}^{-0.5}\,\dot{\bar{\rho}} \tag{2}$$

$$\dot{\bar{\rho}} = A(1-\bar{\rho})\left|\dot{\varepsilon}_p\right| - C\bar{\rho}^{\eta_2} \tag{3}$$

$$\dot{\omega} = \eta_1 \dot{\varepsilon}_p{}^{\eta_2}/(1-\omega)^{\eta_3} \tag{4}$$

$$\sigma = E(1-\omega)\left(\varepsilon_T - \varepsilon_p\right) \tag{5}$$

In this equation set, Eq. (1) represents the viscoplastic flow rule of material, where $\dot{\varepsilon}_p$ is the plastic strain rate, σ is the flue stress, ω is the damage factor, n is the viscosity exponent, and

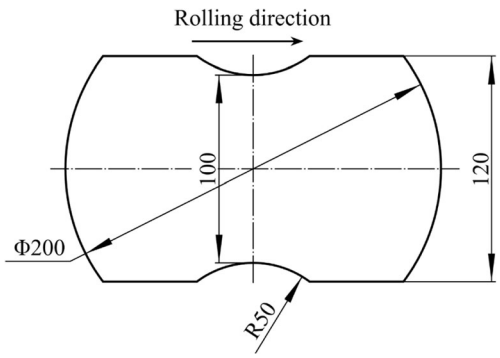

Fig. 3 Dimension of the specimen for the hot formability tests

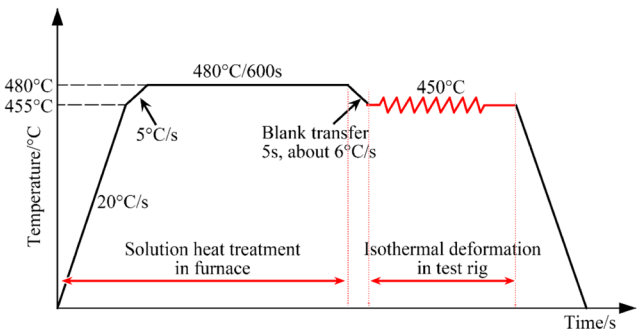

Fig. 4 Temperature profile of hot formability tests

R is the hardening coefficient, which is expressed as a function of normalized dislocation density, $\overline{\rho}$ [19], as shown in Eq. (2). The detailed explanation of normalized dislocation density was illustrated by Lin et al. [20]. Eq. (3) represents the evolution of normalized dislocation density, the first term represents working hardening and the second term represents recovery during deformation. Eq. (4) represents the damage evolution. In the uniaxial hot forming condition, damage factor ω is related to strain rate and deformation temperature. It is assumed that, the damage factor equals to zero at the initial state of the material and accumulates with the proceeding of deformation. When 70% of the cross-section area was damaged, i.e. $\omega = 0.7$, it is assumed that failure occurs. Eq. (5) represents the Hook's law, the effective flue stress is corrected by damage factor for plastic deformation.

In this equation set, K, k, A, B, C, n, η_1, η_2, and E are temperature dependent material constants defined in Eq. (6) [21], and n_2, η_3 are temperature independent constants.

$$\begin{cases} K = K_0 exp\left(Q_K \middle/ RT\right) \\ k = k_0 exp\left(Q_k \middle/ RT\right) \\ B = B_0 exp\left(Q_B \middle/ RT\right) \\ C = C_0 exp\left(-Q_C \middle/ RT\right) \\ A = A_0 exp\left(-Q_A \middle/ RT\right) \\ n = n_0 exp\left(-Q_n \middle/ RT\right) \\ E = E_0 exp\left(Q_E \middle/ RT\right) \\ \eta_1 = \eta_{10} exp\left(-Q_{\eta_1} \middle/ RT\right) \\ \eta_2 = \eta_{20} exp\left(Q_{\eta_2} \middle/ RT\right) \end{cases} \tag{6}$$

3.2 Establishment of multi-axial CDM damage model

For hot stamping aluminum alloy thin sheets, plane stress assumption is normally used as the normal stress in the thickness direction is assumed as zero. The stress state and strain path of material varies with the proceeding of deformation which requires to extend the above uniaxial model to a multi-axial model [22]. Hence, a multi-axial CDM material model, proposed by Lin et al. [17], was utilized considering effects of effective stress, maximum principal stress and hydrostatic stress on the damage. Therefore, the damage formulation based on the plane stress state were established to replace the damage equation for uniaxial case.

The relationship between multi-axial flow rule and uniaxial flow rule can be described as Eq. (7) according to the dissipation function [17]:

$$\dot{\varepsilon}_{ij}^{p} = \frac{3}{2}\frac{S_{ij}}{\sigma_e}\dot{\varepsilon}_{e}^{p} \tag{7}$$

Where $\dot{\varepsilon}_{ij}^{p}$ is the plastic strain rate tensor, $\dot{\varepsilon}_{e}^{p}$ is the effective plastic strain rate, σ_e is effective stress, S_{ij} is the deviatoric stress tensor.

Considering the plane stress state effect, the damage equation of Eq. (4) need to be modified to Eq. (8)

$$\dot{\omega} = \frac{\Delta}{(\alpha_1+\alpha_2+\alpha_3)^{\varphi}}\left(\frac{\alpha_1\sigma_1 + 3\alpha_2\sigma_H + \alpha_3\sigma_e}{\sigma_e}\right)^{\varphi} \left(\eta_1 \dot{\varepsilon}_p{}^{\eta_2}/(1-\omega)^{\eta_3}\right) \tag{8}$$

Where σ_1, σ_H, and σ_e represent maximum principal stress, hydrostatic stress and effective stress, respectively, α_1, α_2, and α_3 are corresponding weighting parameters, representing the contribution of each stress parameter on the damage. φ is a plane-stress damage exponent, representing the effect of plane-stress state on damage evolution. Δ is the correction factor representing the measurement error of necking between uniaxial tensile tests and formability tests [17].

Finally, the CDM unified damage constitutive equations extended from the uniaxial damage constitutive equations can be summarized as:

$$\begin{cases} \dot{\varepsilon}_{e}^{p} = \left(\frac{\sigma_e/(1-\omega)-R-k}{K}\right)^{n} \\ \dot{\varepsilon}_{ij}^{p} = \frac{3}{2}\frac{S_{ij}}{\sigma_e}\dot{\varepsilon}_{e}^{p} \\ \dot{R} = 0.5B\bar{\rho}^{-0.5}\dot{\bar{\rho}} \\ \dot{\bar{\rho}} = A(1-\bar{\rho})|\dot{\varepsilon}_p| - C\bar{\rho}^{n_2} \\ \dot{\omega} = \frac{\Delta}{(\alpha_1+\alpha_2+\alpha_3)^{\varphi}}\left(\frac{\alpha_1\sigma_1 + 3\alpha_2\sigma_H + \alpha_3\sigma_e}{\sigma_e}\right)^{\varphi}\left(\eta_1 \dot{\varepsilon}_p{}^{\eta_2}/(1-\omega)^{\eta_3}\right) \\ \sigma_{ij} = E_{ijkl}(1-\omega)\left(\varepsilon_{ij} - \varepsilon_{ij}^{p}\right) \end{cases} \tag{9}$$

Where E_{ijkl} is the material elastic matrix.

3.3 Analysis of the material constitutive model

Material constants of the uniaxial damage model were determined using a Genetic Algorithm (GA) based optimization methodology [23] by fitting hot uniaxial tensile test results in Section 2.2, and the obtained constants are given in Table 2.

Table 2 Determined values of material constants in uniaxial material model

Fig. 5 shows the comparison of computed material model fitting (solid curves) and experimental true stress strain results (symbols). As can be seen in this figure, the flow stress increases with increasing strain rate due to strain harding, and decreases with increasing temperature due to decrease of yield stress [17]. Flow stress decreases dramatically at the end of deformation due to the damage softening. Good agreement between model fitting and experimental results was achieved.

Table 2 Determined values of material constants in uniaxial material model

K_0 (MPa)	k_0 (MPa)	B_0 (MPa)	C_0 (s^{-1})	E_0 (MPa)	Q_K (J/mol)
1.050	0.224	1.5	3968	3892	21910
Q_k (J/mol)	Q_B (J/mol)	Q_C (J/mol)	Q_E (J/mol)	Q_A (J/mol)	Q_n (J/mol)
21300	25580	14910	13269	50123	5755
A_0	n_0	n_2	η_{10}	η_{20}	Q_{η_1}
9868	11.5	1.8	1.23	0.885	11020
Q_{η_1}	η_3				
622	8.8				

Fig. 6 shows effects of deformation temperature and strain rate on the damage evolution. It can be seen from this figure that damage accumulated with the increase of true strain. Initially, damage factor equals to 0, indicating that the material is homogeneous without damage. Then, the damage accumulates with increasing true strain due to the nucleation and growth of micro-cracks occurs simultaneously [24]. Finally, with the coalescence of micro damage to microcrack, damage factor rapidly increases to 0.7 at the ultimate tensile strain, indicating the failure of material. In Fig. 6a, at a constant temperature 450 °C, the rapid increase of damage occurred in a smaller strain at a lower strain rate 0.1 s^{-1} compared with that of 10 s^{-1}. Similarly, in Fig. 6b, at a constant strain rate 1 s^{-1}, the rapid increase of damage occurred in a smaller strain at a higher temperature 500 °C compared with that of 400 °C. Similar trends can be found in reference [4].

As illustrated in [17], the determination of material constants for the damage parameters of the extended CDM material model requires experimental FLC data for AA7075 in hot stamping condition. In this study, an offset methodology proposed by Mohamed et al. [25] was utilized. Firstly, the material constants governing the FLC shape was obtained by fitting the FLC at room temperature. In this fitting, the temperature-dependent material constants were converted to temperature-independent to switch off viscoplastic feature of aluminum alloys in hot stamping condition. Then, the

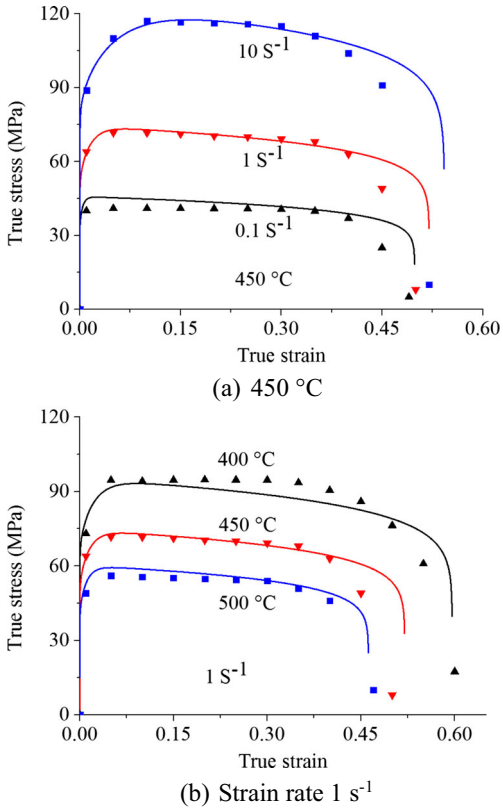

Fig. 5 Comparisons of the hot uniaxial tensile results (symbols) and material model fitting (solid curves) for different temperatures and strain rates.

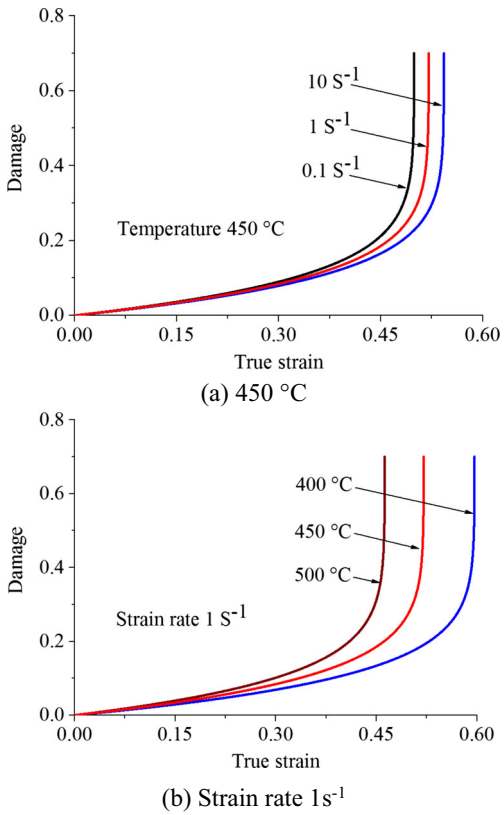

Fig. 6 Effect of deformation temperature (a) and strain rate (b) on the damage factor evolution.

Table 3 Material constants for plane stress damage parameters

Δ	α_1	α_2	α_3	φ
0.6	0.4	-0.04	0.05	8

obtained constants,Δ, α_1, α_2, α_3, and φ were used combining those constants determined by hot uniaxial tensile results. Finally, the constants of multi-axial material model were obtained, and the established material model can be used to predict FLCs for different temperatures and strain rates.

Using this offset method, Table 3 gives the values of FLC of AA7075 for cold stamping [26]. Fig. 7 shows the comparison of computed (solid curves) and the experimental (symbol dots) FLC results for AA7075 at room temperature, and the predicted FLCs for different temperatures and strain rates. It can be seen form this figure that good agreement was achieved, indicating a good prediction accuracy of the CDM model. Fig. 7a shows that the FLCs have been elevated with decreasing deformation temperature from 500 °C to 400 °C. This phenomenon was in consistent with the uniaxial tensile experimental result, which has a larger ultimate tensile strain in the temperature 400 °C. Fig. 7b shows that the FLCs have been elevated with increasing strain rate from 0.1s^{-1} to 10 s^{-1}, even though the effect of strain rate on the shape of FLCs was very small.

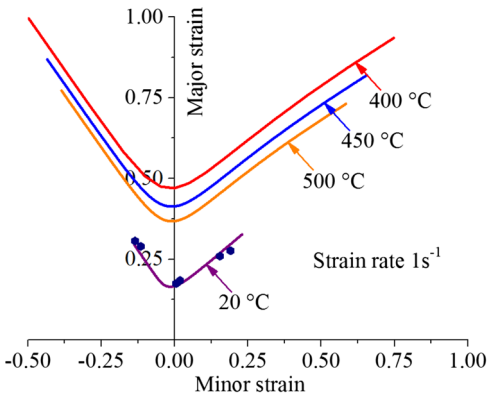

(a) Strain rate 1s^{-1}

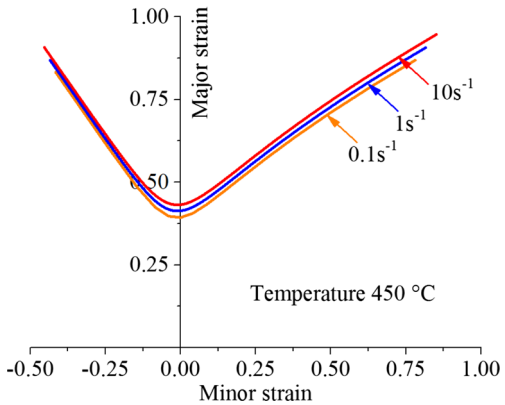

(b) 450 °C

Fig. 7 Predicted FLCs of AA7075 for different temperatures and strain rates in hot stamping condition

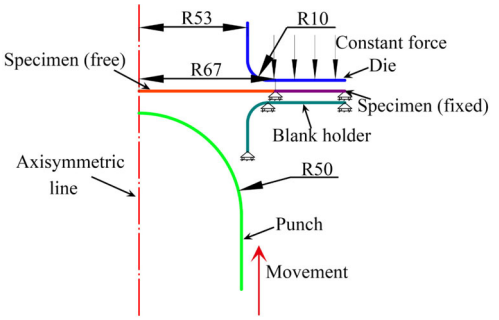

(a) Schematic of the FE model

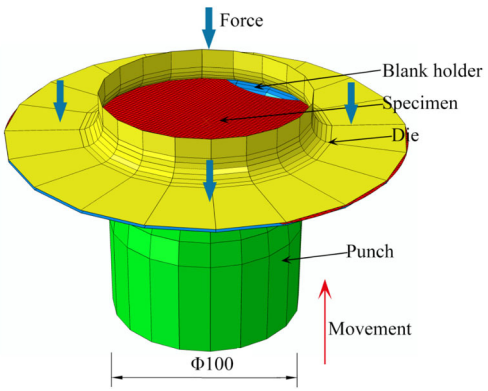

(b) Simulation mesh

Fig. 8 FE model and simulation test rig for the hot formability test

Table 3 Material constants for plane stress damage parameters

4 FE model and simulation set-up

To further investigate hot formability of AA7075, finite element simulations were performed using software ABAQUS/Explicit. Material model and strain hardening model are defined by the developed CDM constitutive equations, which are implemented in ABAQUS software via user-defined subroutine VUMAT. Fig. 8 shows the FE model and simulation test rig of hot formability tests. The geometry and dimensions in this FE model was consistent with the experimental test rig in Section 2.3.1. Tools were modelled as analytic rigid bodies to improve the simulation efficiency considering the huge strength difference between cold die and hot blank, while specimen was modelled as a deformable plastic body. The specimen was meshed using S4RT thin shell elements with five integration points in the thickness direction, and there was a total of 6400 elements. Mises yield criterion was used.

In the FE model, specimen was divided into two regions. In the region with a radius of 63mm, blank material was free to be deformed. While for the region with a radius greater than 63mm, blank was fixed to act as draw bead used in the

experiment to improve simulation efficiency. Friction coefficient between aluminum sheet and punch was set as 0.1 [27], while friction coefficient for aluminum sheet clamped by the blank holder and die was set as 0.3. Coulomb friction model with the penalty formulation was selected as the interface friction model. Blank holder force was set as 20 KN to restrict the material flow into the die cavity. Temperatures of tools and blank were set at 400, 450, and 500 °C, respectively. Considering the isothermal feature of hot formability tests, heat transfer between tools and blank was ignored, only thermal radiation and thermal convection to the environment temperature were considered. The punch speed was set to 20 mm/s.

5 Result and discussions

5.1 FE validation

The developed FE model was validated by normalized thickness and strain distributions. The normalized thickness $\bar{t}$, is equal to t/t_0, where t is the thickness after deformation and t_0 is the intital blank thickness. The thickness values were measured from a symmetric line of a cross-section sectioned across the center at the rolling direction, as indicated in Fig. 9a, using digital vernier caliper. Fig. 9a shows the comparison of normalized thickness distribution between experimental results (solid symbols) and computed results (solid lines). These results were obtained from simulated shape and experimental part with a punch stroke of 35 mm. The stamping speed was 20 mm/s and the used friction coefficient was 0.1.

Besides the comparison of normalized thickness distribution, maximum strain was also used to validate the FE model. Grid automatic analysis software AutoGrid was used to analyze the maximum strain along the symmetric line. Fig. 9b shows the comparison of maximum strain of simulated and experimental parts at a punch stroke of 50 mm with a friction coefficient of 0.1, and the used stamping speed was 20 mm/s. It can be seen from the figure that thickness distribution and maximum strain distributions of the two parts was were in good correlation. Hence, the developed FE model was accurate enough to reflect the deformation characteristics of hot formability tests, and to be used further investigate effects of process variables on the material deformation.

(a) Comparison of normalized thickness distribution of a hot formed part, where solid symbols represent experimental results and solid curve represents computation results
(b) Maximum strain verification for the FE model

Fig. 9 FE model verification

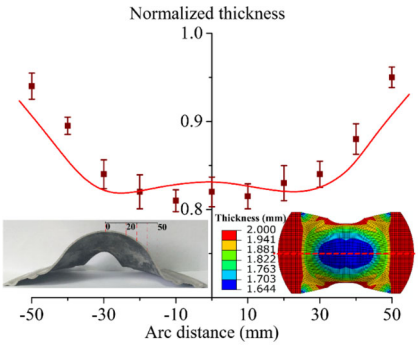

(a) Comparison of normalized thickness distribution of a hot formed part, where solid symbols represent experimental results and solid curve represents computation results

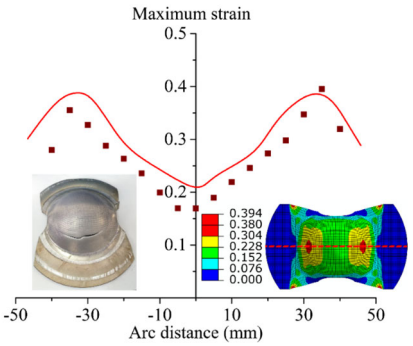

(b) Maximum strain verification for the FE model

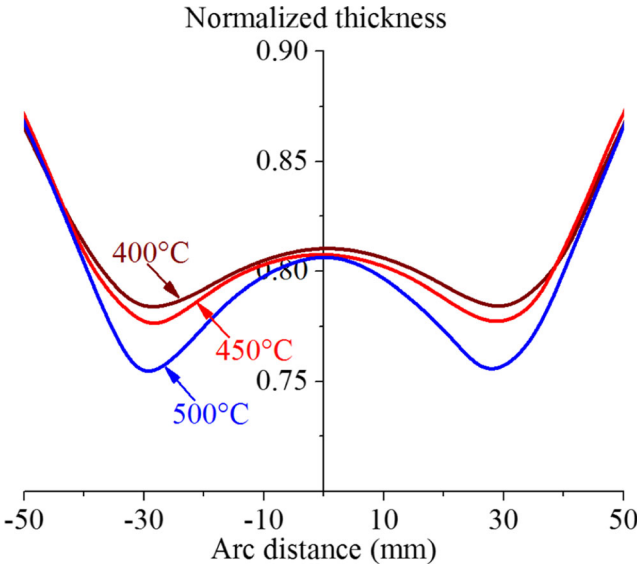

Fig. 10 Effect of temperature on the thickness distribution (400 °C, 450 °C, 500 °C)

5.2 Process variables effect

Fig. 10 shows the effect of temperature (400 °C, 450 °C, 500°C) on the thickness distribution within the deformation zone at a punch speed 20 mm/s and friction coefficient 0.1. These results were obtained from simulated part with 45 mm punch stroke. It can be seen from this figure that minimum thickness occurred at a distance, about 30 mm in the arc length, from the specimen center due to the effect of friction [28]. Localized thinning occurred approximately at the same positions for all temperatures. By changing temperature form 400 °C to 500 °C, the minimum thickness decreased from 1.56 mm to 1.51 mm, and the punch stroke decreased from 53mm to 45mm. Meanwhile, thickness uniformity under 400 °C was better than that at a higher temperature. For AA7075, the damage factor was temperature sensitivity, this made the damage factor accumulated earlier at a higher temperature. Furthermore, material is stronger and strain hardening effect is greater at lower temperatures. Hence, the deformation of AA7075 after SHT in hot stamping can obtain a better formability at a lower temperature.

Fig. 11 shows the effect of punch speed (20 mm/s, 100 mm/s, 200 mm/s) on the thickness distribution at a temperature of 500 °C and friction coefficient of 0.1. These results were obtained from simulated part with 45 mm punch stroke. It can be seen from this figure that the trend of thickness distribution in the center zone (-35mm<arc distance<35mm) was the same for all speeds, while the thickness distribution in the region with arc distance greater than 35mm was overlapped. Localized thinning occurred approximately at the same position with arc distance of 30mm. The slope of linear fitting for maximum strain and deformation time is considered as the strain rate, and strain rates corresponding to punch speed 20 mm/s, 100 mm/s, and 200 mm/s are 0.19 s^{-1}, 0.93 s^{-1}, and 1.86 s^{-1}, respectively. Since strain hardening effect was greater at a faster strain rate, higher strain rate was better to improve formability of AA7075. With increasing punch speed from 20 mm/s to 200 mm/s, punch stroke increased from 45mm to 48mm, and minimum thickness increased from 1.51mm to 1.56mm. Therefore, the formability under punch speed 200 mm/s was better than that under 20 mm/s and 100 mm/s, indicating that formability of AA7075 was better at higher punch speed.

Fig. 12 shows the effect of friction coefficient (0.01, 0.1, 0.3) on the thickness distribution at a punch speed of 20 mm/s and temperature of 500 °C. These results were obtained from

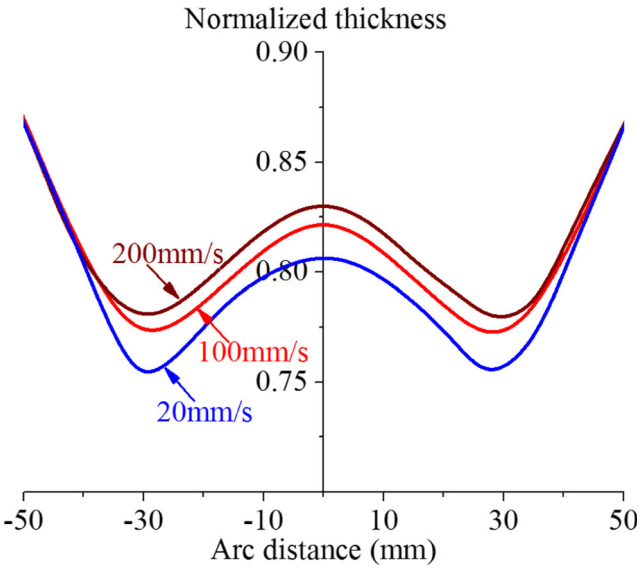

Fig. 11 Effect of punch speed on the thickness distribution (20 mm/s, 100 mm/s, 200 mm/s)

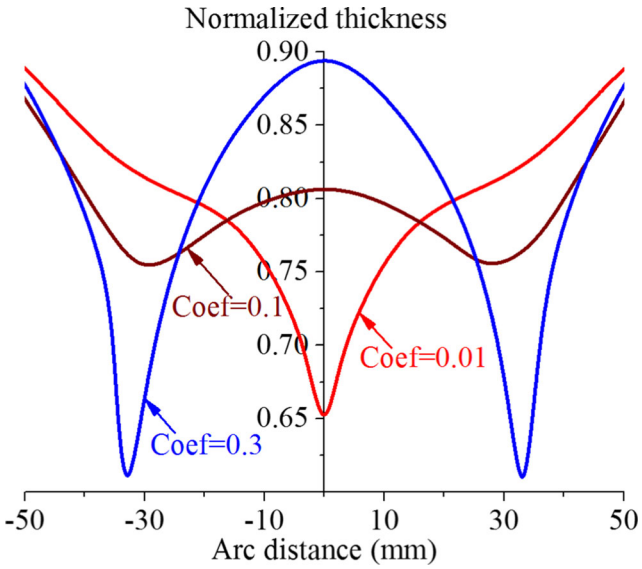

Fig. 12 Effect of friction coefficient on the thickness distribution (0.01, 0.1, 0.3)

simulated part with 45 mm punch stroke. In the condition of friction coefficient 0.01, the maximum localized thinning occurred in the center of the specimen, with a minimum thickness of 1.30mm. While in the condition of friction coefficient 0.3, the maximum localized thinning occurred at a distance of 35 mm from the center of the specimen, with a minimum thickness of 1.22mm. Location of the maximum localized thinning moved from the center of specimen to the outer edge with increasing friction coefficient from 0.01 to 0.3, which indicates that the location of necking can be affected by friction. Furthermore, maximum punch stroke was also affected by the friction coefficient. Maximum punch strokes under friction coefficient from 0.01 to 0.3 were 43mm, 45mm, and 41mm, respectively, formability under friction coefficient of 0.1 was the best of the three. Meanwhile, thickness uniformity under friction coefficient of 0.1 was better than that at 0.01 or 0.3. Therefore, it can be concluded that formability in hot stamping condition was affected by friction coefficient, a reasonable friction coefficient can be used to improve the formability.

5.3 Computed damage evolution

Fig. 13a shows the computed results for damage evolution of aluminum sheet at different locations during deformation at a temperature of 500 °C. The used friction coefficient was 0.1, and punch speed was 20 mm/s. Normalized time T/T_f was used to express different time moments during deformation, where T represents the current time and T_f represents the final deformation time. At the beginning of deformation, the damage factor was zero, which represents the perfect microstructure without damage in the material. Then, with the occurrences of nucleation, growth, and coalescence of microdamage during deformation [15], damage factor in the aluminum sheet gradually grew linearly ($T/T_f < 0.5$). At the time $T/T_f = 0.3$, the maximum damage was only 0.013, which occurred near the center of the specimen. With increasing deformation time, damage accumulated and maximum damage factor gradually moved from the center of specimen to the periphery of the specimen due to the friction effect. At last, at the distance of 30mm to the center of the specimen, the damage factor rapidly grew to 0.7, indicating necking was experienced at this location.

Fig. 13b shows the computed results for damage distribution along the symmetric line at different moments. At the time $T/T_f = 0.8$ and $T/T_f = 0.9$, the maximum damage factor of the specimen was only 0.093 and 0.136, respectively, far below the necking criteria, damage factor equaling to 0.7. Furthermore, it can be found that just before the failure of material ($0.9 < T/T_f < 1$), a small increase of deformation resulted in a significant increase of damage factor, and the increase of damage factor during the later deformation time ($0.9 < T/T_f < 1$) was much larger than that during earlier deformation time ($0 < T/T_f < 0.9$). It can be concluded that, once necking was experienced at a specific location, localized deformation was concentrated there and quickly developed to crack. Hence, for hot stamping, blank deformation should be controlled within uniform deformation range before necking.

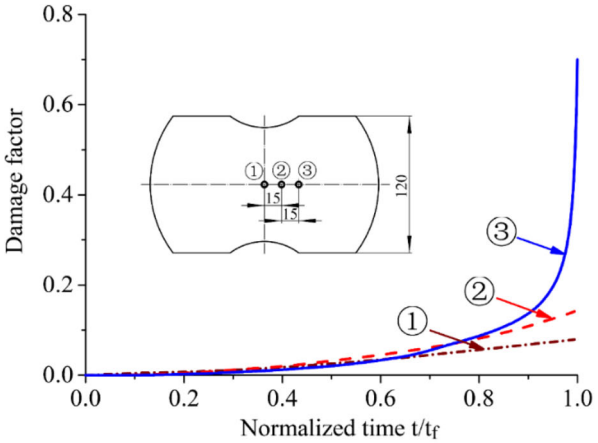

(a) Damage evolution for different positions

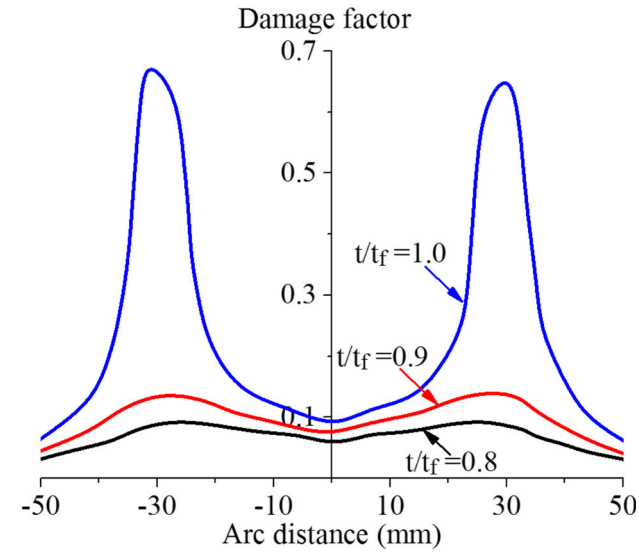

(b) Damage distribution at different deformation time

Fig. 13 Computed damage evolution (temperature of 500 °C, friction coefficient 0.1, and punch speed of 20 mm/s)

6 Conclusion

Based on the above results in this paper, a series of conclusions can be drawn as follows:

(1) The hot uniaxial tensile test results have shown that, the formability was improved with decreasing deformation temperature and increasing strain rate in hot stamping condition.

(2) A set of CDM unified damage constitutive equations for hot stamping AA7075 was established based on hot uniaxial tensile test results.
(3) A FE model with the implemented CDM model was established and validated by corresponding results.
(4) Process variables effects were numerically investigated using developed FE model. The formability was improved with decreasing forming temperature and increasing forming speed. In addition, friction has a dominant effect on determining failure location.

Acknowledgement This work was supported by the Joint Funds of the National Natural Science Foundation of China (grant number U1564202). The authors are grateful to Professor Jianguo Lin of Imperial College London for guidance in genetic algorithm-based optimization.

References

1. Liu YJ, Liu Y, Chen JN (2015) The impact of the Chinese automotive industry: scenarios based on the national environmental goals. J Clean Prod 96:102–109. doi:10.1016/j.jclepro.2014.05.015
2. Wang A, Zhong K, El Fakir O, Liu J, Sun C, Wang L, Lin J, Dean TA (2017) Springback analysis of AA5754 after hot stamping: experiments and FE modelling. Int J Adv Manuf Tech 89:1339–1352. doi:10.1007/s00170-016-9166-3
3. Fakir OE, Wang L, Balint D, Dear JP, Lin J, Dean TA (2014) Numerical study of the solution heat treatment, forming, and in-die quenching (HFQ) process on AA5754. Int J Mach Tool Manu 87:39–48. doi:10.1016/j.ijmachtools.2014.07.008
4. Mohamed MS, Foster AD, Lin J, Balint DS, Dean TA (2012) Investigation of deformation and failure features in hot stamping of AA6082: Experimentation and modelling. Int J Mach Tool Manu 53:27–38. doi:10.1016/j.ijmachtools.2011.07.005
5. Foster A, Dean TA, Lin J (2013) Process for forming aluminium alloy sheet components. European Patent, EP2324137
6. Wang L, Strangwood M, Balint D, Lin J, Dean TA (2011) Formability and failure mechanisms of AA2024 under hot forming conditions. Mat Sci Eng A 528:2648–2656. doi:10.1016/j.msea.2010.11.084
7. Zhou J, Wang B, Lin J, Fu L (2013) Optimization of an aluminum alloy anti-collision side beam hot stamping process using a multi-objective genetic algorithm. Arch Civ Mech Eng 13:401–411. doi:10.1016/j.acme.2013.01.008
8. Ablat MA, Qattawi A (2016) Numerical simulation of sheet metal forming: a review. Int J Adv Manuf Tech:1-16. doi:10.1007/s00170-016-9103-5
9. Zhang J, Deng Y, Zhang X (2013) Constitutive modeling for creep age forming of heat-treatable strengthening aluminum alloys containing plate or rod shaped precipitates. Mat Sci Eng A 563:8–15. doi:10.1016/j.msea.2012.10.055
10. Liu G, Zhang GJ, Ding XD, Sun J, Chen KH (2003) Modeling the strengthening response to aging process of heat-treatable aluminum alloys containing plate/disc- or rod/needle-shaped precipitates. Mat Sci Eng A 344:113–124. doi:10.1016/S0921-5093(02)00398-2
11. Worswick MJ, Chen ZT, Pilkey AK, Lloyd D, Court S (2001) Damage characterization and damage percolation modelling in aluminum alloy sheet. Acta Mater 49:2791–2803. doi:10.1016/S1359-6454(01)00163-X
12. Shi D, Hu P, Ying L (2016) Comparative study of ductile fracture prediction of 22MnB5 steel in hot stamping process. Int J Adv Manuf Tech 84:895–906. doi:10.1007/s00170-015-7754-2
13. Xu F, Lin J, Zhao S, Zhang H (2016) Research of the Gurson damage model of the different yield functions during the deep-drawing process. Int J Adv Manuf Tech:1-17. doi:10.1007/s00170-016-9873-9
14. Wu B, Li MQ, Ma DW (2012) The flow behavior and constitutive equations in isothermal compression of 7050 aluminum alloy. Mat Sci Eng A 542:79–87. doi:10.1016/j.msea.2012.02.035
15. Ma W, Wang B, Bian J, Tang X, Yang L, Huo Y (2015) A New Damage Constitutive Model for Thermal Deformation of AA6111 Sheet. Metall Mater Trans A 46:2748–2757. doi:10.1007/s11661-015-2823-6
16. Lin J, Dean TA (2005) Modelling of microstructure evolution in hot forming using unified constitutive equations. J Mater Process Tech 167:354–362. doi:10.1016/j.jmatprotec.2005.06.026
17. Lin J, Mohamed M, Balint D, Dean TA (2013) The development of continuum damage mechanics-based theories for predicting forming limit diagrams for hot stamping applications. Int J Damage Mech 23:684–701. doi:10.1177/1056789513507731
18. Shao Z, Li N, Lin J, Dean TA (2016) Development of a new biaxial testing system for generating forming limit diagrams for sheet metals under hot stamping conditions. Exp Mech 56:1489–1500. doi:10.1007/s11340-016-0183-9
19. Garrett RP, Lin J, Dean TA (2005) An investigation of the effects of solution heat treatment on mechanical properties for AA 6xxx alloys: experimentation and modelling. Int J Plasticity 21:1640–1657. doi:10.1016/j.ijplas.2004.11.002
20. Lin J, Liu Y, Farrugia D, Zhou M (2005) Development of dislocation-based unified material model for simulating microstructure evolution in multipass hot rolling. Philos Mag 85:1967–1987. doi:10.1080/14786430412331305285
21. Mohamed MS, Lin J, Wang L, Balint D (2013) Hybrid forming processes for production of lightweight high strength automotive panel parts. International Heat Treatment and Surface Engineering 4:160–165. doi:10.1179/174951410x12851626813014
22. Mohamed M, Shi ZS, Lin JG, Dean TA, Dear J (2015) Strain-based continuum damage mechanics model for predicting FLC of AA5754 under warm forming conditions. Applied Mechanics and Materials 784:460–467. doi:10.4028/www.scientific.net/AMM.784.460
23. Cao J, Lin J (2008) A study on formulation of objective functions for determining material models. Int J Mech Sci 50:193–204. doi:10.1016/j.ijmecsci.2007.07.003
24. Bieler TR, Eisenlohr P, Roters F, Kumar D, Mason DE, Crimp MA, Raabe D (2009) The role of heterogeneous deformation on damage nucleation at grain boundaries in single phase metals. Int J Plasticity 25:1655–1683. doi:10.1016/j.ijplas.2008.09.002
25. Mohamed M, Lin J, Foster A, Dean TA, Dear J (2014) A New Test Design for Assessing Formability of Materials in Hot Stamping. Procedia Engineering 81:1689–1694. doi:10.1016/j.proeng.2014.10.214
26. Yang XY, Lang LH, Liu KN, Cai GC, Guo C (2015) Prediction of forming limit diagram of AA7075-O aluminum alloy sheet based on modified M-K model. Journal of Beijing University of Aeronautics and Astronautics 41:675–679
27. Foster AD, Mohamed MS, Lin JG, Dean TA (2008) An investigation of lubrication and heat transfer for a sheet aluminium Heat, Form-Quench (HFQ) process. Steel Res Int 79:113–120
28. Bai Q, Mohamed M, Shi Z, Lin J, Dean TA (2016) Application of a continuum damage mechanics (CDM)-based model for predicting formability of warm formed aluminium alloy. Int J Adv Manuf Tech 88:3437–3446. doi:10.1007/s00170-016-8853-4